100-kHz Interferometric Rayleigh Scattering Flow Diagnostics at 266 nm

Andrew D. Cutler[1]
George Washington University, Washington, DC 20052, USA

Naibo Jiang[2], Sukesh Roy[3]
Spectral Energies, Dayton, OH 45431, USA

Paul M. Danehy[4]
NASA Langley Research Center, Hampton, VA 23681, USA

Interferometric Rayleigh scattering (IRS) is a laser-based technique capable of spatially and temporally resolved measurement of gas velocity and temperature in unseeded gaseous flows. In the present embodiment of the technique, IRS is performed at 266 nm for the first time. IRS at 266 nm is potentially much less susceptible to interferences from particles and other stray light sources. A pulse-burst laser and high-speed camera provided image rates of 100 kHz, allowing simultaneous space- and time-resolved measurement in high speed flow at multiple points along a line. The use of 266 nm excitation and detection is compared with prior work that used 532 nm. New experimental interferogram modelling and fitting techniques for single and multi-velocity-component IRS were demonstrated in a study of the spatial and temporal variation of the flow along a line through a supersonic jet. Single component velocity and temperature measurements using 266 nm were successfully made and compared with prior 532 nm results. Two-component velocity measurements at 266 nm, using the reflected image method, were compared to single-component measurements.

I. Introduction

The interferometric Rayleigh scattering (IRS) set of techniques are laser-based, optical techniques that enable the measurement of velocity, and potentially temperature and density in a gas flow without requiring particle or gaseous seeds. Velocity sensitivity arises out of sensitivity to Doppler shift, temperature sensitivity arises through the scattering linewidth, and density through the absolute scattering signal level. For flows at density greater than atmospheric the Rayleigh scattering line shape becomes sensitive to pressure as well as temperature, so there is potential that IRS could be used for direct pressure measurement. Non-intrusive techniques such as IRS are suitable for high-speed flows where physical probes may not tolerate the environment or where they may alter the flow they seek to measure. IRS has found application to high speed jets,[1,2,3,4,5] wind tunnels, and high-speed combustion flows[6,7] where flow-related changes in Mach number, temperature and pressure are relatively high. Both nanosecond pulsed lasers [1,5,6,7] and narrow linewidth CW lasers[2,3,4] have been employed in IRS systems.

In a typical implementation of the pulsed-laser IRS technique, Rayleigh scattered light from a region of interest of the flow field is collected by a (collection) lens and collimated, passed through a Fabry-Perot interferometer (etalon), and focused by a second (imaging) lens to form an image (interferogram) on a camera, as illustrated in Figure 1. The etalon consists of a pair of parallel mirrors which are partially reflective. Fixed gap etalons are especially suitable for

[1] Professor, Department of Mechanical and Aerospace Engineering, AIAA Associate Fellow.
[2] Senior Research Scientist, AIAA Associate Fellow.
[3] Senior Research Scientist, AIAA Associate Fellow.
[4] Senior Technologist, Advanced Measurements and Data Systems Branch, AIAA Associate Fellow.

IRS as they are less snesitive to the effects of vibration that adjustable gapped etalons. There are two types of fixed gas etalon: a solid etalon, which is typically a fused silica plate with flat parallel mirrored surfaces, and a fixed-gap air-spaced etalon which consists of a pair of flat parallel plates, mirrored surfaces inward. The gap between the parallel plates of a fixed-gap air-spaced etalon is maintained by pillars fabricated from a low coefficient-of-thermal-expansion glass, and is much less sensitive to effects of temperature variation than a solid etalon. Collimated light rays passing through the etalon and the imaging lens at a given angle relative to the optical axis all focus to a given point on the camera sensor. With the etalon removed, all these rays would have the same optical path length to the sensor and interference is constructive. With the etalon replaced, interference occurs at this focus between light that has taken optical paths of different lengths due to multiple reflections in the etalon. At certain angles, dependent on the wavelength of the light, the different path lengths are integer multiples of the wavelength and interference is constructive, forming bright rings in the interferogram, at other angle interference is destructive. The interferogram (top right in Figure 1) is thus built up by rays passing through the etalon at different angles to the optical axis.

Rayleigh scattering in the flow of interest is generated by a focused laser beam – for best signal, the electric field of the laser beam is perpendicular to the plane of the incident and scattered light vectors, $\vec{k}_0$ and $\vec{k}_s$. Diffuse, uniformly distributed laser light scattered from a surface behind the laser beam may also be collected. This background scattering is neither Doppler shifted nor broadened and can provide a reference signal with which the Rayleigh scattering from the laser beam can be compared. The appearance of the background scattering in the interferogram is of concentric bright rings, and the appearance of the focused laser beam is of a narrow horizontal band of bright "patches" overlapping or adjacent to the rings, corresponding to the laser beam. Since the scattering from the laser beam is broadened due to the Rayleigh line and shifted by the Doppler effect, the patches within the horizontal band (the laser beam image) are radially broadened and shifted relative to the rings. Gas temperature and a component of velocity can be inferred by analyzing these interferograms.

One disadvantage of IRS is that the etalon typically rejects 96%-99% of the light that would otherwise reach the sensor. Higher laser beam pulse energy or higher gas density may be required than in other Rayleigh-scattering-based techniques for good signal. Quite high laser pulse energies are available with ns pulsed lasers, but peak power at the laser beam focus is often enough to cause laser-induced breakdown of the gas, which destroys the IRS signal and perturbs the flow. Use of a pulse stretcher to lengthen the laser pulse from ~10 ns to ~100 ns can provide a factor of four increase in pulse laser energy before breakdown.[5] A related technique to IRS, interferometric "Mie" scattering, [8] uses the same or similar instrument but depends on scattering from small (<< 1 micron) condensate particles rather than Rayleigh scattering. This technique potentially provides higher signal and narrower scattering linewidth, and consequently higher accuracy of velocity measurement, but temperature measurement from linewidth is not possible. Suitable condensate fogs occur naturally in high speed wind tunnels if the relative humidity in the test gas is increased.

IRS configurations that enable simultaneous measurement of multiple orthogonal components of velocity have been proposed by Bivolaru.[5,6] Two possibilities provide for a relatively simple optical system. In the reflected image method, light scattered in the 180° position relative the optical axis is reflected by a concave mirror to form a virtual image of the laser beam that is displaced a little above the original laser beam. This virtual image is inverted left-to-right. The interferogram thus contains both virtual image and original laser beam. The Doppler shift of the Rayleigh scattering from the laser beam viewed directly is proportional to the u_1 component of velocity while the Doppler shift of the scattering in the 180° direction, i.e., from the virtual image, is proportional to the u_2 component. In the reflected beam method, the laser beam is reflected 180° and refocused just above the first focus of the laser beam; the Doppler shift of the scattering from the reflected laser beam is proportional to the u_2 component of velocity. A downside of the reflected beam method is that the two components of velocity are measured at different spatial locations whereas in the reflected image method provides simultaneous measurement of two orthogonal velocity components at the same points in space. IRS configurations that enable two-dimensional mapping of flow parameters, as opposed to one-dimensional along a focused laser beam, include use of multiple focused laser beams created by a microlens array,[9] which also uses reference background light, and use of a laser sheet, in which the reference background is replaced in the analysis by an interferogram acquired with the flow turned off.[1] These methods require higher laser energy or stronger scattering media (e.g. scattering from high pressure gas, heavy gas or Mie particles) compared to the single focused beam used in the present work.

Analysis of pulsed laser interferograms in some prior work[5,6,7] involves several steps. The first is to find the center of the interferogram rings. The second is to map the interferogram from x, y space to radial (i.e., distance from the ring center), y space. The third is to map the radial coordinate to optical frequency. The fourth is to bin pixel signal

intensity in y to provide a spectrum (intensity versus frequency) for each order (ring number) of the superimposed Rayleigh scattered and background light. The resulting spectra are fitted to the summation of a Gaussian model for the Rayleigh scattering spectrum and a Lorentzian model for the background scattering to determine Doppler shift, which is the frequency difference between the centers of the Rayleigh and the background spectra. A method for measurement of temperature was proposed[7] in which a second leg was added to the IRS system that imaged a reference cell, and collimated Rayleigh scattered light collected from the focused laser beam in the flow and a focused laser beam in the reference cell were merged prior to the imaging lens and camera. Temperature and density in the flow were inferred by referencing the linewidth and intensity of the Rayleigh scattering in the flow to the linewidth in the cell (where temperature and density were known). This method was demonstrated in a Hencken burner flame. In more recent work,[10,11] a conceptually simpler approach for interferogram analysis is adopted in which a theoretical model of the interferogram is developed that has among its parameters the flow parameters of interest, including velocity and temperature; the measured interferogram is fitted to the model via an iterative procedure that minimizes the residual between measured and theoretical interferogram. This method has the advantage that all the factors that determine the interferogram, both physical and experimental (such as image blurring in the detector) can be directly modelled in an intuitive way. The method was applied in the mapping of velocity and temperature distributions in an underexpanded sonic jet.[10,11]

It is often useful to resolve fluid motions in time. If statistics of flow unsteadiness in a statistically stationary flow, such as the standard deviation, are to be measured accurately it is enough that pulse lengths be shorter that any time scales of flow unsteadiness. If it is important to resolve velocity variation in time, the pulses need additionally to be spaced in time by less than these time scales. While pulse lengths of ns lasers are short in relation to flow time scales, ~10 Hz lasers cannot resolve motion in most flows of practical interest. Development of pulse-burst lasers and high-speed CMOS cameras have enabled data rates of IRS systems to be increased to up to 100 kHz.[10,11] Pulse burst lasers also have the advantage that very high laser pulse energy and tailored pulse lengths up to 100 ns are possible, removing the need to for pulse stretchers to avoid laser induced breakdown. This is a significant advantage because pulse stretchers can be large, time consuming to align and they require maintenance to stay aligned.

All the IRS studies referenced so far used doubled Nd:YAG lasers at 532 nm (excluding CW lasers). However, IRS in the ultraviolet has potential advantages. Rayleigh scattering intensity scales as λ^{-4}, leading to much greater signal for given laser energy. This greater signal generation efficiency results in a much better ratio of signal to scattering interferences by large (>>1 micron) particles, windows, and surfaces, etc. that may occur in wind tunnels and test facilities, which are roughly independent of wavelength. Thus, while energy is lost in converting from 532 nm to 266 nm, the signal intensity is recovered through greater scattering efficiency and the scattering interferences are reduced with laser energy, resulting in increased signal-to-interference ratio.

Laser Rayleigh scattering measurements of density have been previously made in the ultraviolet, for example in [12,13]. The present work describes the first implementation of IRS in the ultraviolet. The same pulse-burst laser, high-speed CMOS camera, and under-expanded sonic jet flow was used as was used in [11]. However, the laser frequency is now quadrupled to 266 nm and the camera now utilizes an intensifier with relay optics. Working with an intensifier has many disadvantages, including non-linearity at high intensity, image blurring, intensifier image noise, lower dynamic range, and greater susceptibility to damage by high light intensity. However, the high-speed camera required is not sensitive to light at 266 nm. The 266 nm IRS system is employed to measure distributions of velocity and temperature in the jet. Both single-component and two component velocity measurements were made, the latter using the reflected image method.

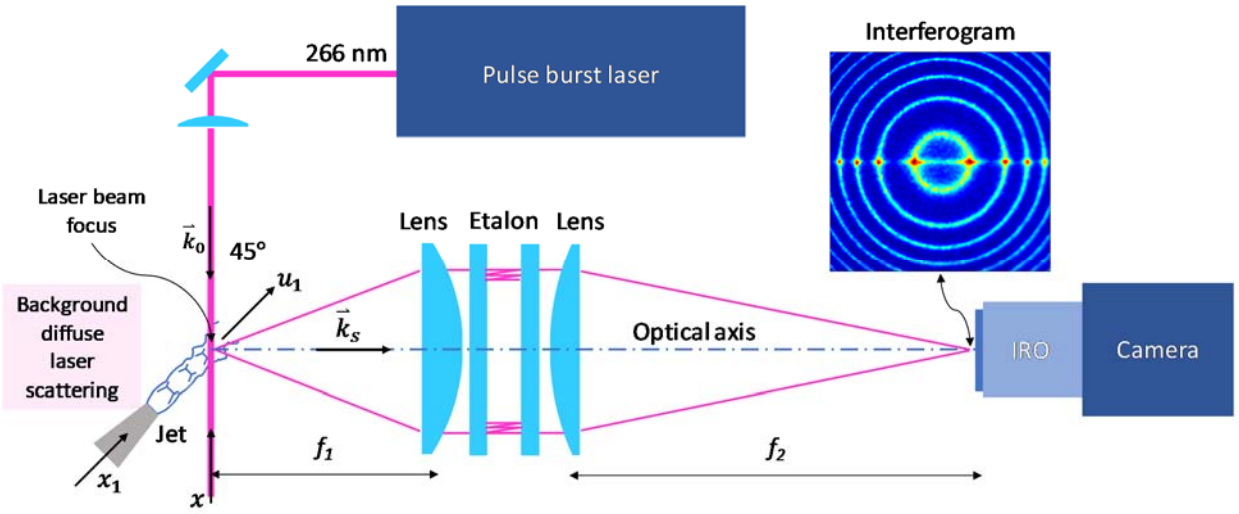


Figure 1 IRS system and high-speed jet flow (not drawn to scale).

II. Interferogram Analysis

The method by which the flow parameters are obtained from the interferogram has been described [11]. The interferogram or a sub-region of it is represented theoretically as a function of parameters of the laser light, the geometry of the focused laser beam, the distribution of background laser scattering, the etalon, and the imaging system. Some of these parameters are well known and the rest are determined by fitting. A residual is defined as the summed squared difference between the measured intensity and the fitted theory at each image pixel. The parameters are found by iterating on them to mininize the residual.

The theoretical interferogram for a given set of parameters is found by first representing the imaged light field by the (incoherent) summation of the background light field, which has the same spectrum as the original laser beam and is uniformly distributed or varies smoothly, and the image(s) of Rayleigh scattering from the focused laser beam. Parameters of the laser beam image include beam width, position, and angle. The transmission of the light through the etalon as it appears in the image on the sensor is given below.

$$\frac{Transmission}{Maximum\ transmission} = \frac{1}{1 + G sin^2(\frac{\delta}{2} + C\pi)} \qquad Eqn.\,1$$

The contrast coefficient G, function δ, and the radial distance r from the intersection of the optical axis with the sensor (the center of the rings).

$$(a)\quad G = \frac{4R_1}{(1-R_1)^2}, \qquad (b)\quad \delta = \frac{4\pi n d}{\lambda}\sqrt{1 - \frac{1}{n^2\left(1 + \left(\frac{f_2}{r}\right)^2\right)}} \qquad Eqn.\,2$$

In these equations R_1 is the reflectivity of the etalon surfaces, n is the refractive index of the material between the etalon mirrors, d is the spacing between the mirrors, and f_2 is the focal length of the imaging lens. In principle, the phase parameter C is any integer. However, uncertainties in δ due to even very small uncertainties in the values of n, λ, and d can be very large. These parameters are typically not fitted individually but specified approximately, and any subsequent error is corrected by fitting a non-integer value of C.

To derive the total transmission through the etalon, intensity is numerically integrated with respect to wavelength at to account for laser and scattered linewidth and Doppler shift, as discussed below. Additional broadening of the interferogram to account, for example, for image blurring by the camera intensifier, is accomplished by convolving it with a Gaussian function.

The laser beam is centered at the nominal laser wavelength λ_{laser} and its' spectrum is modelled by a Gaussian function with a frequency full-width-half-maximum (FWHM) of $\Delta\nu_{laser}$. The background scattering has the same spectral characteristics as the laser beam while the Rayleigh scattered light is broadened relative to the laser beam. For air at

density greater than atmospheric this broadening is thermally dominated with a Gaussian line shape and a frequency linewidth FWHM given by:

$$\Delta\nu_{Rayleigh} = \frac{4}{\lambda_{laser}}\sin\left(\frac{\theta}{2}\right)\sqrt{2\ln(2)R_{gas}T} \qquad Eqn.\ 3$$

In this equation, θ is the viewing angle, the angle between the scattered and incident light vectors $\vec{k}_s, \vec{k}_0$, and is 90° in the current experiment. The other parameters are the (mass-specific) gas constant R_{gas} and the temperature T. For air at atmospheric density or greater the line shape depends upon both thermal and acoustic processes and is called the Cabannes line.[14] The lineshape can be approximated by the Tenti S6 model, which depends upon the temperature, viewing angle, pressure p, laser wavelength, and the gas composition.[15] In the present study the pressure is taken to be constant at one atmosphere, Matlab functions for modelling the Tenti S6 line are from [16], and gas property modeling is from [17]. In addition to line broadening, if the gas is flowing then Rayleigh scattering is Doppler shifted by a frequency of:

$$\Delta\nu_{Doppler} = \frac{(\vec{k}_s - \vec{k}_0).\vec{u}}{2\pi} = \frac{\sqrt{2}\,u_1}{\lambda_{laser}} \qquad Eqn.\ 4$$

Note that both the Rayleigh line width and Doppler shift are inversely proportional to the laser wavelength: both increase by a factor of two going from the green to the ultraviolet. The second equality of Eqn. 4 applies only for the geometry of Figure 1 where the observation angle is 90°.

III. System Design Considerations

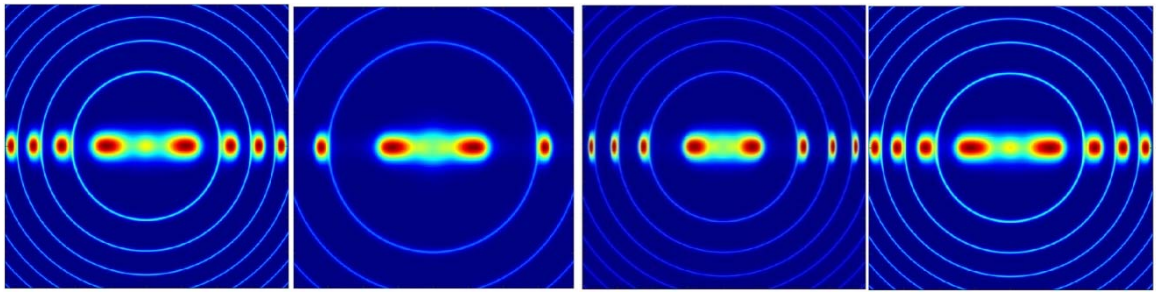
Design and optimization of an IRS system requires an understanding of the interplay of various parameters that govern the spacing of the rings in the ring pattern, the spectral sensitivity (defined below), the magnification of the image, and the image intensity. While it is desired to optimize these parameters, many of these must be traded off against each other. Peak transmission of the etalon at a given light frequency occurs at regular phase intervals separated by $\delta = \pm 2\pi$ (Eqn 1). For small light ray angles to the optical axis it follows from Eqn. 2(b) that the interval in frequency corresponding to this interval in phase is given below (c is the speed of light):

$$\Delta\nu_{FSR} = \frac{c}{2nd} \qquad Eqn.5$$

This frequency change is known as the free spectral range (FSR) and for a given etalon mirror spacing it is independent of the wavelength of the light. The transmission of diffuse monochromatic light through the etalon thus appears in the image as a series of bright rings that will shift radially as the frequency changes, and the original pattern is repeated when the frequency is shifted by $\pm\Delta\nu_{FSR}$. An etalon for IRS is typically selected so that the Rayleigh scattering line width and Doppler shift are less than the FSR, to avoid overlapping transmission of lines from adjacent orders, but not much less, to obtain good resolution of the spectrum. For example, for 266 nm laser light at ambient conditions the Rayleigh scattering linewidth is approximately 3.7 GHz. An etalon with FSR of 10 GHz will result in non-overlapping spectra. Small angle analysis of Eqn 2(b) and substitution of Eqn. 5 provides the characteristic radius at which the phase changes by -2π from the optical axis, i.e., the frequency is raised by one FSR, given by Eqn 6(a). The spectral sensitivity, defined as the rate of change of radius on the sensor of the etalon peak transmission frequency, is found by Eqn. 6(b), which is derived by small angle analysis.

$$(a) \quad r_{char} = f_2\sqrt{\frac{\lambda_{laser}n}{d}} = nf_2\sqrt{\frac{2\Delta\nu_{FSR}\lambda_{laser}}{c}} \qquad (b) \quad \left(\frac{\partial r}{\partial \nu}\right)_{n,d,f2} = \frac{n^2 f_2^2 \lambda_{laser}}{c\,r} \qquad Eqn.6$$

Selecting an air-spaced etalon (n = 1) with FSR of 10 GHz, a wavelength of 266 nm, and an imaging lens focal length of 0.5 m gives r_{char} = 2.1 mm. The simulated interferogram for an 8 mm square sensor, atmospheric air, and a Doppler shift of 3 GHz may be seen in Figure 2(a). Consistent with Eqn. 6(a), if the wavelength is increased a factor of two (FSR, λ_{laser}, f_2 are 10 GHz, 532 nm, 0.5 m) then the characteristic radius is increased by a factor of $\sqrt{2}$, as shown in Figure 2(b). But, if the focal length of f_2 is also reduced by a factor of $\sqrt{2}$ (10 GHz, 532 nm, 0.353 m), as shown in Figure 2(c), or if the FSR is also reduced a factor of two (5 GHz, 532 nm, 0.5 m) then the ring pattern is unchanged relative to (a), as shown in Figure 2(d). Consistent with Eqn. 6(b) the spectral sensitivity in Figure 2(c) is the same as (a) while for (b) and (d) it is doubled. However, per Eqns. 3 and 4 the Doppler linewidth and the Doppler shift (for given velocity) for Figure 2(a) is twice that for (b-d). In other words, while the selection of etalon determines the reference ring spacing, the selection of etalon does not affect the product of spectral sensitivity and Doppler shift/linewidth, which determines the displacement/broadening of the transmission patches on the sensor relative to the rings.



(a) (b) (c) (d)

Figure 2 Simulated IRS interferograms as the focal length of the imaging lens, laser frequency, and etalon FSR are changed.

The transmission lineshape of the etalon is a Lorentzian function (in phase space) with the ratio of frequency linewidth FWHM to the FSR given by the reciprocal of the finesse, defined as $\pi/-\ln(R_1)$. Typically R_1 is set between 80% and 90% (R=84.1%, used in the present work, gives a finesse of 18.1). If the finesse is too low then spectral resolution is poor and if the finesse is so high that that the theoretical line width on the sensor is narrower than camera lens and sensor resolution then signal level is poor (high reflectivity rejects too much light). The etalon mirror gap uniformity and wedge should be less than $\sim\lambda_{laser}/100$ to avoid significant unmodelled/uncontrolled line broadening. The collection lens controls the system magnification via the equation $M = f_2/f_1$. Sensor signal level in number of photons per pixel, N_{pp}, is:

$$N_{pp} \propto I_s \left(\frac{D h_p}{f_2}\right)^2 \qquad Eqn.7$$

In this equation, I_s is the Rayleigh scattering intensity, *D is* the etalon or lens system aperture diameter (whichever is smaller), and h_p is the pixel height. Since f_2 will typically be set to ensure adequate resolution of the interferogram (Eqn. 6), then for a given sensor the signal level can only be increased by increase of the system aperture, which is typically limited by the etalon. It is not possible to circumvent this constraint on the etalon while maintaining system magnification fixed aperture by introducing telescopes into the collimated signal beam to decrease and increase the beam size. The signal intensity level is not affected by the collection lens focal length. However, if f_1 were doubled, which would halve the image magnification, then the focused laser beam would appear half the height in the image and consequently the total number of laser beam photons incident on the sensor would be reduced by a factor of two. It is likely that to maintain system precision the laser energy would need to be doubled.

Measurement of flow parameters by an IRS system is likely to be more accurate if the product (spectral sensitivity of the system) × (Doppler shift for given flow velocity or Rayleigh scattering linewidth) is high. This product at given radius on the sensor is not dependent on the selection of laser wavelength or etalon but is proportional to (focal length of the imaging lens)^2. The number of rings on the sensor, which determines to the amount of information on the interferogram and the ability to analyze it, is proportional to (focal length of the imaging lens)$^{-1}$ × (FSR × laser wavelength)$^{-0.5}$.

Measurement of flow parameters by an IRS system is also likely to be more accurate if the signal-to-noise ratio at the sensor is high. If the spectral sensitivity × Doppler shift is kept constant, i.e., the focal length of the imaging lens is kept constant, then signal level is proportional to laser energy × (system aperture diameter)^2. Pulse-burst laser systems have the advantage of narrow laser line width and are capable of very high laser pulse energies distributed over 20 ns or longer, mitigating laser breakdown issues associated with beam focusing and providing high signal levels. The reference rings are created by surface scattering, so noise will include laser speckle, which is likely to become larger than photon shot noise as laser energy is increased. Laser speckle may also be important for Rayleigh scattering from small particles that are too large to follow the thermal molecular motion (such as small droplets and condensates).[14] Speckle size scales with the Airy disc which is proportional to (laser wavelength) × (focal length of the imaging lens) / system aperture. The effect of laser speckle is minimized if the Airy disc size is small. Thus, it is desirable for the system aperture (defined by the etalon) to be high. Selection of etalon finesse is also important as it determines transmission of scattered light onto the sensor. The etalon linewidth should be of similar size to the spatial resolution of the sensor or the size of the imaging lens focal spot, whichever greater.

IV. Experiment

A. Experiment Setup

The laser and optical system for 100 kHz IRS at 266 nm is described – see also Figure 1. The focused laser beam is generated by a pulse-burst laser system manufactured by Spectral Energies LLC. The laser provides up to 1000 pulses per 100 kHz burst with nominal 40 mJ/pulse at 532 nm that is doubled to 4 mJ/pulse at 266 nm. The approximately 6 mm diameter beam is focused with a nominally 300-mm focal-length lens to a focus of 60-100 micron FWHM diameter. A scattering plate is placed behind the laser beam, in the field of view of the camera, and dispersed laser light is projected onto it to generate the reference background scattered laser light. The collection lens has a nominally 100 mm focal length and is uncoated. It is mounted in a three-component stage so it can be aligned to be approximately on the axis of the imaging lens, and so it could be set one focal distance from the laser beam. An air-gapped etalon is employed that has a free spectral range of 9.99 GHz, a gap spacing and surface flatness within $\lambda/100$ at 266 nm, a mirror reflectivity of 84.1%, and a 30-mm clear aperture. The image is formed by a single plano-concave fused silica lens with nominal focal length of 0.5 m (actual focal length of f_2 =0.47 m) that in combination with the collection lens provides a system with magnification of ×5. The spot size of the singlet lens is comparable to the calculated diffraction-limited spot size for the etalon aperture. The sensor was a Phantom Fastcam SA-Z camera with 20 μm pixels that was set up with a 384×384-pixel field of view and image acquisition rate of 100 kHz. An intensifier was necessary since the available high-speed camera is not sensitive at 266 nm without an intensifier. A LaVision lens-coupled intensifier was employed with nominal magnification of ×1.

An under-expanded high-speed jet flow is generated from a gas bottle via a convergent nozzle. The exit internal diameter is 2.48 mm and the nozzle exterior is tapered at a shallow angle to a sharp edge at the exit. The jet is pointed obliquely toward the focus of the laser beam at 45° to the beam axis (see Figure 1) and the distance along the jet axis from the nozzle exit to the laser beam is 14.7 mm. Rayleigh scattered light from the focus is collected at 90° to the laser beam by the IRS system located on the opposite side of the laser beam from the nozzle. The configuration is such that the Doppler shift of the Rayleigh scattered light collected by the IRS system was from the component of velocity parallel to the jet flow axis. Tests with flow were at supply pressure set to 100 psia. The jet could be scanned in a motion parallel to the laser beam. This jet flow was profiled using IRS at 266 nm as described herein and was previously studied using 532 nm IRS as described in [11].

B. Results

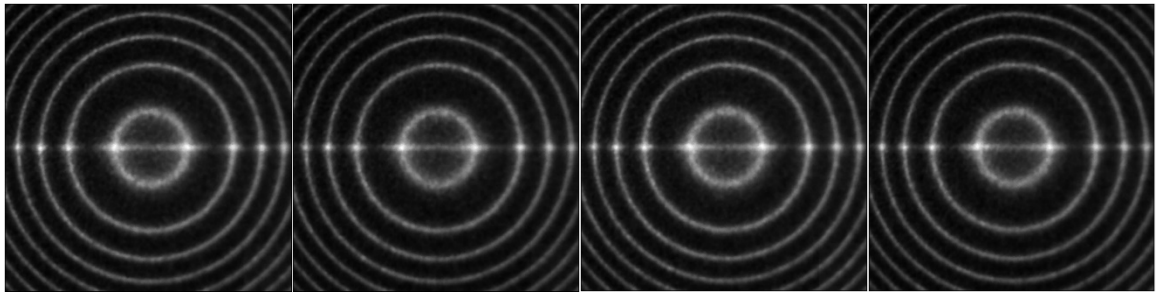


Figure 3 Set of 4 consecutive interferograms with no flow.

Figure 3 shows four consecutive interferograms of a pulse burst measured in ambient air. These show clearly the expected reference rings, which is the etalon filtered image of the background scattered laser light, with horizontal line of patches approximately through the center of the rings, which is the etalon-filtered image of the laser beam. The general impression is that these images are identical to each other, other than image noise, consistent with stable laser frequency. A preliminary fit of a sequence of 100 interferograms from this laser pulse burst is performed to obtain the unknown geometrical, camera, and laser parameters of the setup. It is typically necessary to continue to fit the diameter and position of the focused beam as these parameters change during a pulse-burst due to thermal lensing of the laser. The phase parameter, C, which is related to the laser frequency and mirror spacing, is also fitted. This parameter does not change measurably during a pulse-burst, consistent with a fixed laser frequency and etalon mirror spacing but may change over longer periods of time. The results of such a fit for a single interferogram (one laser pulse) at ambient conditions (nominal zero velocity and 293 K) are shown in Figure 4. In Figure 4(a) is the

measurement, (b) is the fit to a portion of the measurement, and (c) is the difference between the fit and the measurement. The presence of only random noise in the fit region of the difference image, i.e., without coherent structure, indicates a good fit. The fitted blurring FWHM due to the intensifier and relay optics is 73 μm and the fitted laser linewidth is 1.2 GHz. Note that it is possible to fit both these parameters because the broadening by laser linewidth is a constant proportion of the spacing between the rings, which decreases radially outwards, while the blurring is uniform across the interferogram, so these variables are independent. The broadening inherent in the etalon, which has an effect similar to laser linewidth, is well understood theoretically and verified using the same etalon and laser at 532 nm. The fitted velocity is -5.6 m/s and the fitted temperature is 327 K. These discrepancies relative to the actual values of 0 m/s and 293 K give an idea of the bias error in the measurement.

The laser linewidth of 1.2 GHz at 266 nm was unexpectedly large. Measurements in a similar laser indicate a linewidth of about 110MHz at 1064nm and about 150 MHz after doubling to 532 nm.[18] The ratio of linewidths is a little greater than the expected ratio of square root of 2 from theory that assumes a transform limited laser beam. At 1064 nm the beam is close to transform limited while at 532 nm the beam quality is poorer. Doubling the poorer quality 532 nm beam to 266 nm is expected to produce an even greater ratio of linewidths. This line broadening may have been made worse by working at laser intensity that was not high enough to produce good energy conversion efficiency – efficiency was <10%. This will be investigated in future work.

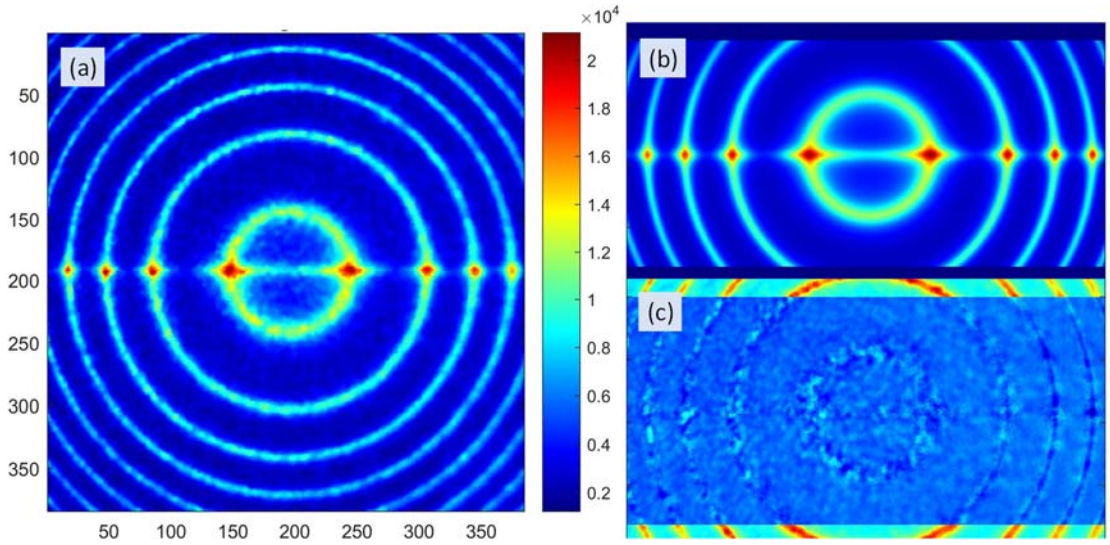


Figure 4 Interferogram at zero velocity: (a) measurement, (b) fit, (c) difference.

Figure 5 shows the results of individually fitting consecutive 100 interferograms of a pulse-burst near the center of the high-speed jet and averaging the results. In this fit, a series of automatically selected rectangular subregions of each interferogram centered around each beam-ring intersection are separately fitted and these individual subregion fits are combined to form a single fit image. The average fits shown are typical for the study of the jet flow in which the jet nozzle was translated to build up a picture of the flow field.

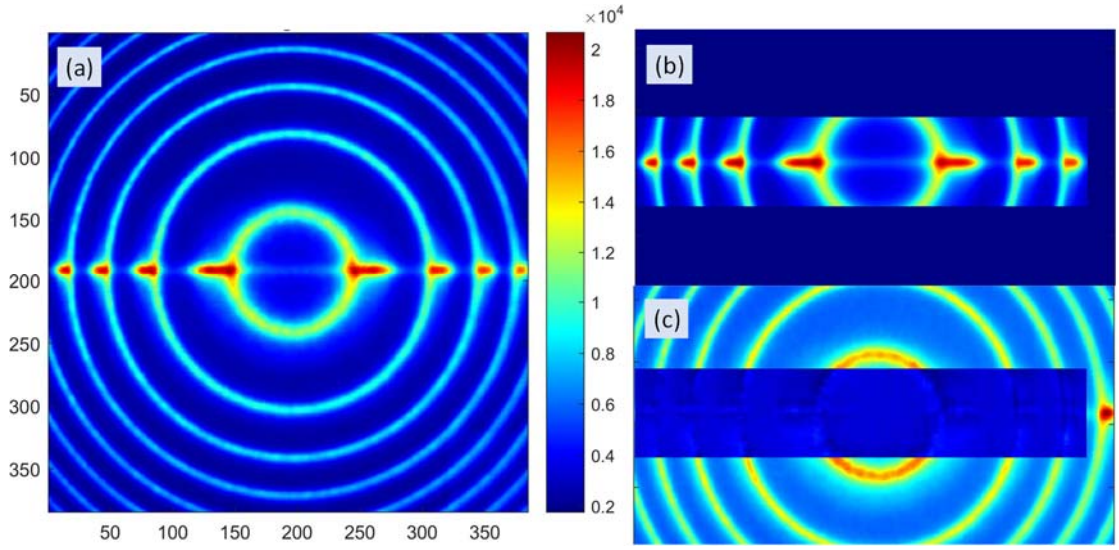


Figure 5 Average of 100 interferograms acquired near the center of the jet: (a) measurement, (b) fit, (c) difference.

Figure 6 shows a comparison of measured intensity to fitted theory for a 9-pixel high horizontal region of the interferogram centered on the beam and averaged vertically. Also shown is a 9-pixel wide vertical region centered on the center of the ring pattern averaged horizontally (capturing reference fringes only). The quality of the fit indicated the horizontal line, fit line, and residual is good; the vertical line, which includes no Rayleigh scattering except close to the center, gives an idea of the laser linewidth and the intensifier broadening, which is substantial.

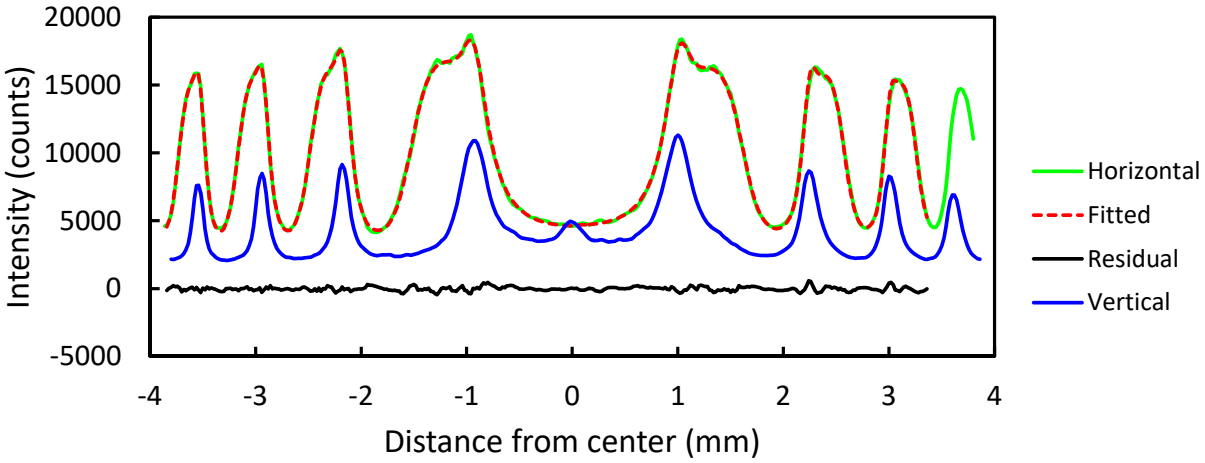


Figure 6 Interferogram intensify averaged across 9-pixel wide bands through the center, one horizontal and one vertical, compared to theory. The residual is fitted minus horizontal.

Figure 7 shows the mean and standard deviation of measured velocity u_1 inferred from a fitting of 100 consecutive individual interferograms of a pulse-burst obtained in the ambient air, plotted as a function of the position on the camera sensor, relative to the center of the rings, around which each fit subregion is located. The difference between the mean velocity and temperature from the nominal expected values of zero and 293 K respectively is a measure of systematic error in the technique, which typically gets worse away from the center of the interferogram. These differences are in the 5-13 m/s range in velocity magnitude and 10-20 K in temperature across most of the interferogram, though are as much as 30 m/s and greater than 30 K at the edge where the spectral sensitivity is less. The standard deviation of the fluctuations is a measure of the single-measurement random error. These standard

deviations are roughly 10 m/s in velocity near the center, rising to 20 m/s at the edge, and are typically 30 K (exceeding 40 K far from the center) in temperature. These errors in velocity are quite similar in magnitude to errors reported at 532 nm in [11], while errors in temperature are roughly 50% higher.

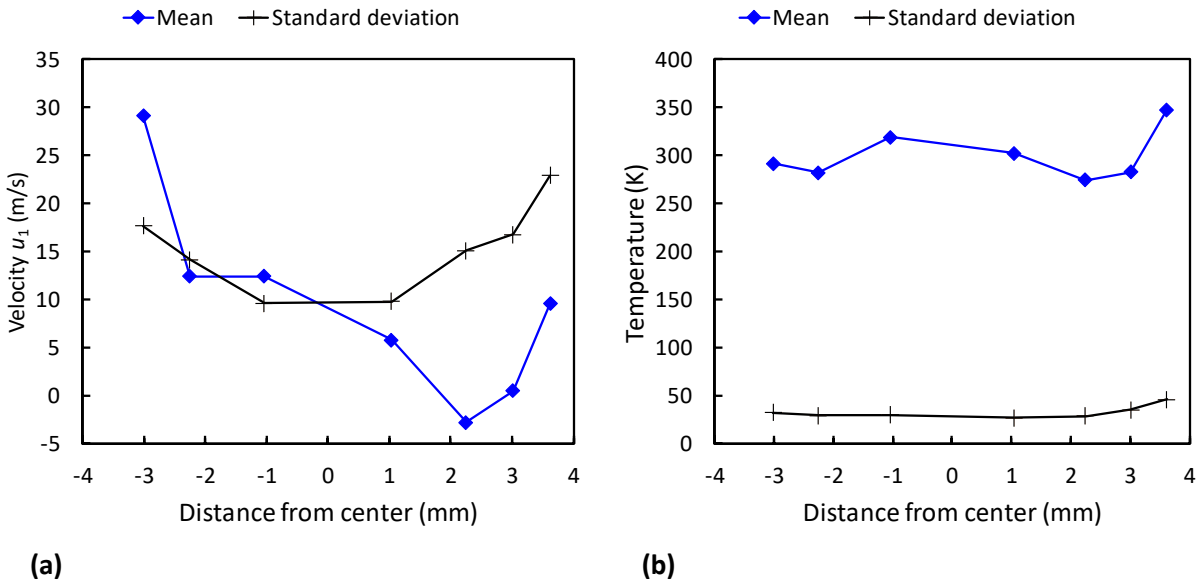


Figure 7 Profiles of mean and standard deviation (a) velocity and (b) temperature in ambient air.

Figure 8 shows the (a) fitted velocity and (b) temperature from 60 consecutive interferograms for two subregions of the interferogram centered around x=1.23 mm and 1.65 mm in the flow (see Figure 1). The fluctuations seen here are significantly greater than the standard deviation observed in the ambient air (no-flow) data, and indicative of real fluctuations in the flow (rather than instrument error). Some correlation between the results at the two locations is indicative of coherent structures that are bigger than the spacing between these points. However, the large differences between consecutive data points are indicative of unsteadiness of time scales greater than 100 kHz.

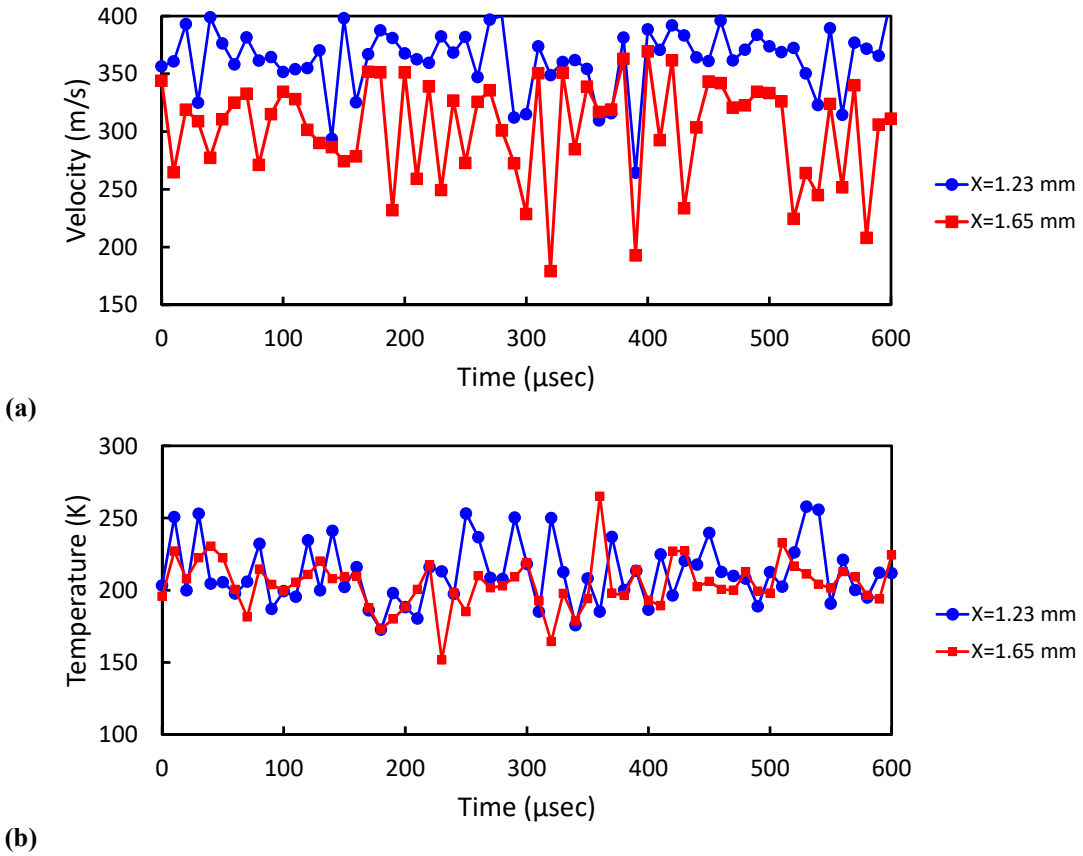
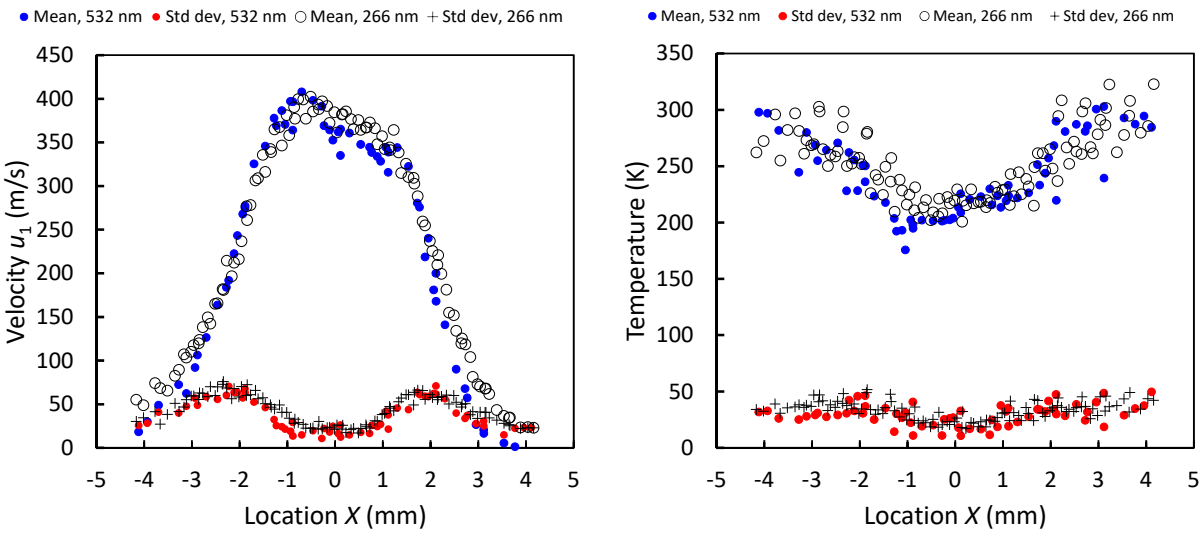


Figure 8 Typical data series in the jet flow (a) flow velocity and (b) flow temperature at x=1.23 mm and 1.65 mm.

Figure 9 shows profiles of the mean and standard deviation of velocity and temperature in the high-speed jet as described herein using 266 nm IRS and compared to measurements using 532 nm IRS from [11]. Using both methods, the jet shows a mean velocity profile that is approximately Gaussian shape but slightly asymmetrical in shape. The asymmetry is because the x_1 axis intersects the optical axis at 45° and the velocity is lower at greater distance from the nozzle exit due to shock interactions. The temperature drops toward the center of the jet due to roughly adiabatic expansion to high velocity from nominally ambient temperature in the nozzle plenum. The velocity and temperature standard deviations peak in the shear layer either side of the jet center where turbulent fluctuations are the greatest. The scatter of the mean velocity and temperature measurements for the 266 nm IRS experiments scatter about their respective trend lines (not shown) by an amount consistent with the errors inferred from the measurements at zero velocity, i.e., approximately ±10 m/s in velocity and ±30 K in temperature. The velocity and temperature distribution trend lines for 266 nm IRS and 532 nm IRS agree with each other within the stated measurement uncertainties and uncertainty in repeating the setup (Measurements occurred on different days with laser beam path and camera lens and intensifier relay optics being changed between measurements).



(a) **(b)**

Figure 9 Scanned profiles of mean and standard deviation (a) velocity and (b) temperature in the jet.

C. Two Component IRS

The reflected image IRS method, illustrated in Figure 10, is used to simultaneously measure two-components of velocity. Light scattered in the 180° direction relative the optical axis is collected and reflected by a concave mirror with center of curvature close to the point in the laser beam being imaged. A reflected virtual image of the laser beam is thus placed a little above the original laser beam. This reflected image of the laser beam, which is inverted left-to-right relative to the original laser beam, is placed so that at the center of the interferogram the location in the laser beam of the direct image and of the reflected image just above it corresponds. The setup is otherwise identical to the setup previously described. The Doppler shift of the Rayleigh scattering from the laser beam viewed directly is proportional to the u_1 component of velocity while the Doppler shift of the scattering in the 180° direction, i.e., from the virtual image, is proportional to the u_2 component. To align the reflected image as described the laser was set to minimum pulse energy and a lens tissue was placed at an oblique angle in the center of the field of view (with camera gain set to 0); both direct and reflected scattering from the point intersection of the tissue with the laser beam focus could then be viewed in the interferogram to establish correspondence.

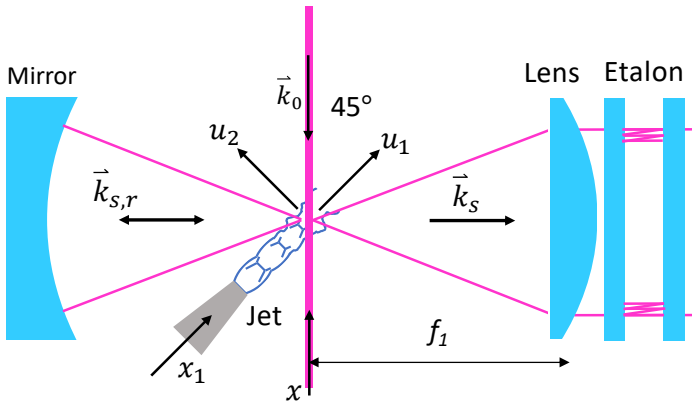


Figure 10 Reflected image method for two-component IRS

Figure 11 shows the results of separately fitting 100 consecutive interferograms obtained during a pulse-burst in ambient air and averaging the results. In these images the top "laser beam" is the reflected image displaced slightly vertically relative the direct view of the laser beam below it. Figure 11(a) is the measured interferogram, (b) is the fit to a portion of it, and (c) is the difference between the fit and the measurement. In this embodiment the background

scattered light is not uniform due to presence of the mirror in the field of view. There may also be interference due to Rayleigh scattered laser light that does not come from the main beam focus. These factors cannot be accurately modeled. The fits in part (b) excluded a narrow region between the direct beam and the reflected image to try to minimize these errors. Within the fitted regions of the interferogram, the magnitude of image intensity differences between fit and measurements are like for the single beam fits. Figure 12 shows the mean and standard deviation of both measured velocity components inferred from a single 100-interferogram sequence obtained in ambient air and plotted as a function of the location on the sensor. Note the approximately two-times greater error both in mean velocity and in standard deviation relative to the known zero velocity as compared to the single beam results. This greater error is attributed to the non-uniform background and interferences discussed above.

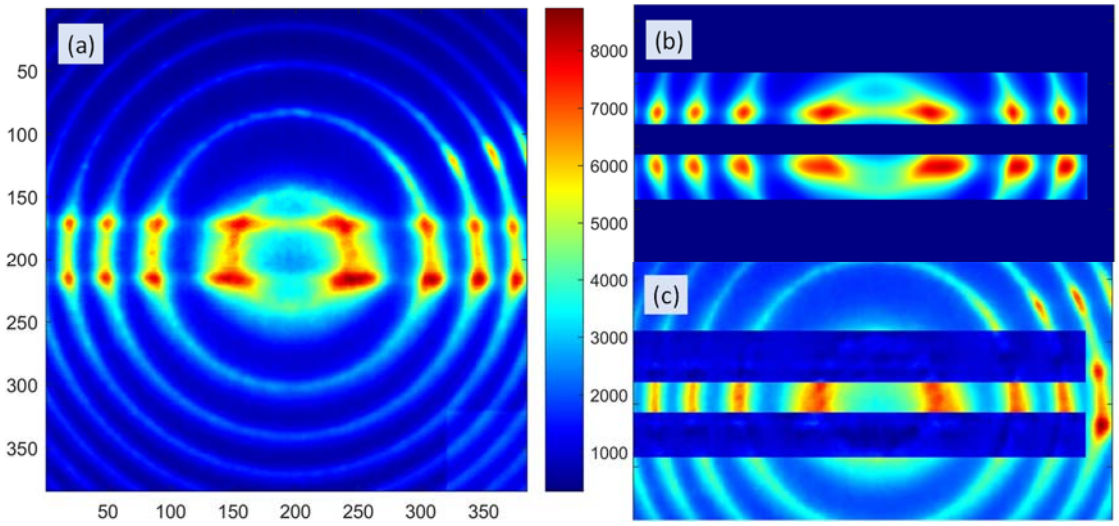


Figure 11 Reflected image interferogram fitting: (a) experiment, (b) fit, (c) difference.

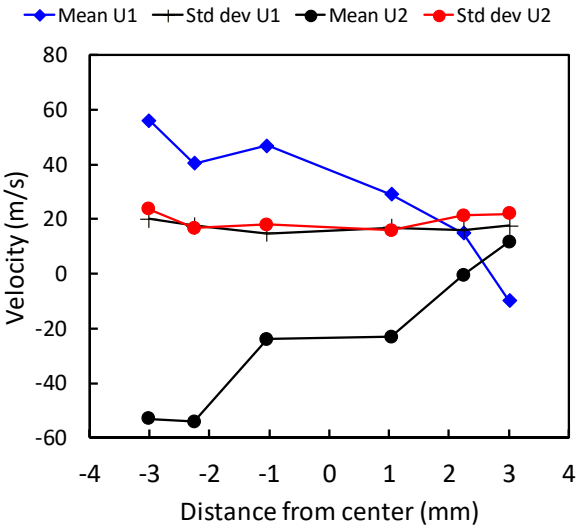


Figure 12 Profiles of velocity at zero velocity using two-component IRS.

Figure 13 shows the two-beam velocity measurements in the jet plotted as a function of the location in the flow. Part (a) compares the u_1 component measured by the two-beam method to the single beam method. Differences in the mean velocity measurements are consistent with the previously noted errors in the ambient air measurement. The standard deviation measurements agree with the single beam measurements. Part (b) shows the u_2 component. The mean is close to zero as expected, but the results have no further significance considering the errors. The standard

deviation is comparable to the ambient air measurement and thus to the measurement error, so the measurement in the jet only provides an upper limit to the actual standard deviation. Thus, the actual standard deviation of u_2 is less than half the standard deviation in u_1, which is consistent with large axial velocity fluctuations in the jet.

It should be possible to mitigate these difficulties associated with the present embodiment of two-beam IRS. Spatial filtering of the laser beam would reduce any stray laser light that is not contained within the laser beam. Issues of mirror interference with the formation of a uniform background using a scattering plate behind the laser beam would not exist in the reflected beam method of IRS (as opposed to the current reflected image method). However, it is expected the reflected image method could be successfully implemented by, instead of generating the background with the scattering plate, relaying laser light via an optical fiber or mirrors, and injecting between the collection lens and etalon.[6,8]

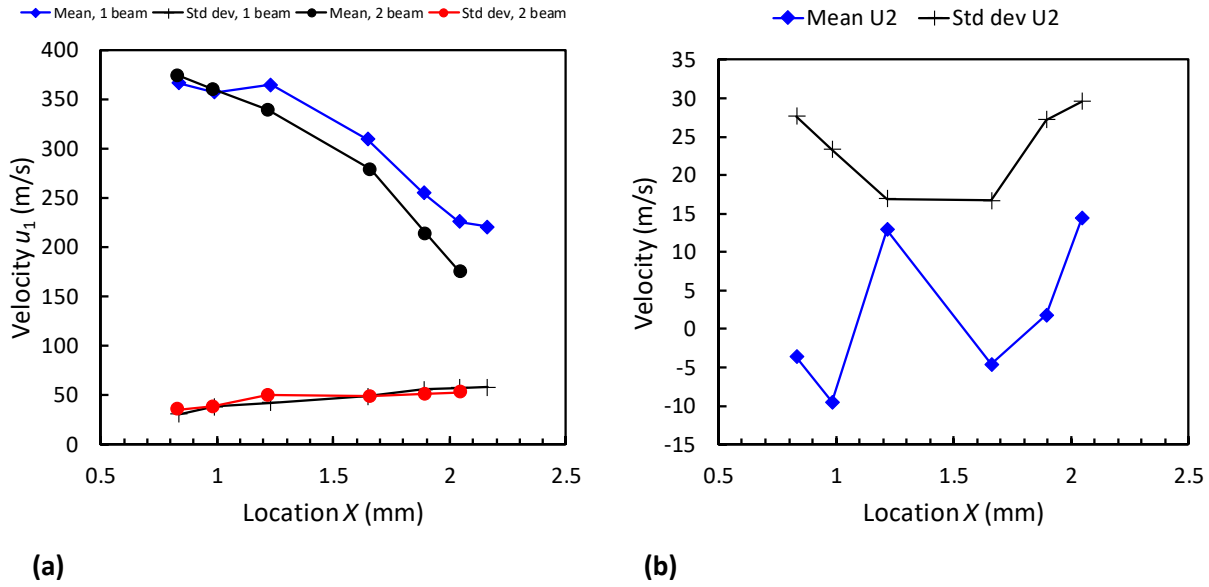


Figure 13 Profiles of velocity in the jet: (a) comparison of two-beam to single-beam measurements of u_1, (b) two-beam measurement u_2.

V. Conclusions

Simultaneous, 100 kHz, multi-point measurements of one and two components of velocity and of temperature at 100 kHz are demonstrated in a small under-expanded sonic jet using an IRS system with a single pulse-burst laser, etalon, and camera. Robust interferogram modeling and fitting methodologies provide good fits to the experimental interferograms. System accuracy is characterized in terms of both bias and random error. The results are compared to recently published experiments at 532 nm that utilize the same laser, camera, and jet flow field. The errors in velocity at 266 nm are like those at 532 nm, while the errors in temperature are roughly 50% greater at 266 nm. The relative errors in temperature are roughly 2× greater than in velocity at both wavelengths. The greater errors are attributed to low laser energy, a broad laser linewidth at 266 nm of 1.2 GHz, and the use of an intensifier and relay optics at 266 nm (which affect signal to noise ratio and cause image blurring). Two-components of velocity are measured using the reflected image method. Errors are higher than for the single-component measurements due to uneven and difficult-to-model background scattering created by the presence of the mirror. Methods for mitigation of these errors are proposed.

Interferometric Rayleigh scattering flow diagnostics has fundamental advantages at shorter wavelengths. The (laser wavelength)$^{-4}$ dependence of Rayleigh scattering provides much greater signal for given laser energy. This dependence provides both greater signal and greater rejection of scattered laser light from surfaces or large particles in the flow, which scattering typically does not depend strongly on wavelength, as might be encountered in a wind tunnel. It is likely that issues of low laser energy conversion efficiency and broad linewidth at 266 nm can be addressed. And, it is noted that a new generation of back-illuminated scientific CMOS cameras can provide good quantum efficiency in the UV, albeit at much lower framing rates. Such developments may be extended to the required high

framing rates in the future. It is therefore conceivable that IRS at 266 nm will prove invaluable for 100 kHz, simultaneous multi-point, multi-flow-parameter measurements in many future aerodynamic testing applications.

Acknowledgments

This work was supported by NASA SBIR 2016 Phase II Solicitation (A1.08 Aeronautics Ground Test and Measurements Technologies) 80NSSC17C0008. Support for PMD provided by the Aeronautics Mission Directorate Transformational Tools and Technologies (TTT) Project.

References

[1] Seasholtz, R.G., "Instantaneous 2D velocity and temperature measurements in high speed flows based on spectrally resolved molecular Rayleigh scattering," AIAA Paper 95-0300, 33rd Aerospace Science Meeting and Exhibit, Jan 9-12, 1995, Reno, Nev. Published Online:22 Aug 2012 https://doi.org/10.2514/6.1995-300

[2] Panda, J., and Seasholtz, R., "Velocity and temperature measurement in supersonic free jets using spectrally resolved Rayleigh scattering," AIAA Paper 99-236, 37th Aerospace Sciences Meeting and Exhibit, Reno, NV, 1999.

[3] Chen, L., Yang, F. R., Su, T., Bao, W. Y., Yan, B., Chen, S., and Li, R. B. (2017). High sampling-rate measurement of turbulence velocity fluctuations in Mach 1.8 Laval jet using interferometric Rayleigh scattering. *Chinese Physics B*, 26(2), 025205.

[4] Mielke, A. F., K. A. Elam, and C.-J. Sung. "Multi-property measurements at high sampling rates using Rayleigh scattering." *AIAA Journal 47*, no. 4 (2009): 850-862.

[5] Bivolaru, D., Danehy, P.M., Lee, J.W., Gaffney, R.L., Cutler, A.D., "Single-pulse, Multi-point Multi-component Interferometric Rayleigh Scattering Velocimeter," AIAA-2006-836, 44th AIAA Aerospace Sciences Meeting, Reno, NV, 9-12 Jan. 2006.

[6] Bivolaru, D., Danehy, P.M., Gaffney, R.L., Jr., and Cutler, A.D., "Direct-View Multi-Point Two-Component Interferometric Rayleigh Scattering System," AIAA 2008-236, 46th Aerospace Sciences Meeting, Reno, NV, Jan 7-10, 2008.

[7] Bivolaru, D., Cutler A.D., and Danehy, P.M, "Spatially- and Temporally-resolved Multi-parameter Interferometric Rayleigh Scattering," AIAA-2011-1293, 49th AIAA Aerospace Sciences Meeting, Orlando, Florida, Jan. 4-7, 2011

[8] Bivolaru, D., -Oslash, M. V., Tzes, A., and Papadopoulos, G. (1999). Image processing for interferometric Mie and Rayleigh scattering velocity measurements. *AIAA Journal*, 37(6), 688-694.

[9] Sheng, Wang, Jin-Hai Si, Shao Jun, Zhi-yun Hu, Jing-feng Ye, and Jing-Ru Liu. "Two-dimensional interferometric Rayleigh scattering velocimetry using multibeam probe laser." *Optical Engineering* 56, no. 11 (2017): 111705.

[10] Estevadeordal, J., Jiang, N., Cutler, A. D., Felver, J. J., Slipchenko, M. N., Danehy, P. M., Gord, J.R., and Roy, S. (2018). High-repetition-rate interferometric Rayleigh scattering for flow-velocity measurements. *Applied Physics* B, 124(3), 41.

[11] Cutler, A.D., Rein, K., Roy, S., Danehy, P.M., Jiang, N., "100-kHz Interferometric Rayleigh Scattering for multi-parameter flow measurements," submitted to *Optics Letters*, 2019.

[12] Balla, R. Jeffrey, and Joel L. Everhart. "Rayleigh scattering density measurements, cluster theory, and nucleation calculations at Mach 10." *AIAA Journal* 50, no. 3 (2012): 698-707.

[13] Balla, R. Jeffrey. "Mach 10 Rayleigh scattering gas-cap density, pressure, and shock-jump measurements." *AIAA Journal* 53, no. 3 (2015): 756-762.

[14] Miles, Richard B., Walter R. Lempert, and Joseph N. Forkey. "Laser Rayleigh scattering." Measurement Science and Technology 12, no. 5 (2001): R33.

[15] Tenti, G., C. D. Boley, and Rashmi C. Desai. "On the kinetic model description of Rayleigh–Brillouin scattering from molecular gases." Canadian Journal of Physics 52, no. 4 (1974): 285-290.

[16] Smith, John, University of Colorado at Boulder, CIRES, October 21st, 2010 https://www.mathworks.com/matlabcentral/fileexchange/29108-coherent-spontaneous-rayleigh-brillouin-scattering-spectra. See also Pan, Xingguo, Mikhail N. Shneider, and Richard B. Miles. "Coherent Rayleigh-Brillouin scattering." *Physical Review Letters* 89, no. 18 (2002): 183001.

[17] Gu, Ziyu, Benjamin Witschas, Willem van de Water, and Wim Ubachs. "Rayleigh–Brillouin scattering profiles of air at different temperatures and pressures." *Applied Optics* 52, no. 19 (2013): 4640-4651.

[18] Jiang, Naibo, Walter R. Lempert, Gary L. Switzer, Terrence R. Meyer, and James R. Gord. "Narrow-linewidth megahertz-repetition-rate optical parametric oscillator for high-speed flow and combustion diagnostics." *Applied Optics* 47, no. 1 (2008): 64-71.